A stochastic study of microsolvation. II. Structures of CO in small helium clusters

F. A. Gianturco[a)]
Department of Chemistry, The University of Rome, Città Universitaria, 00185 Rome, Italy

M. Lewerenz
Zentralinstitut für Angewandte Mathematik Forschungszentrum, Juelich GmbH, D-52425 Juelich, Germany

F. Paesani
Department of Chemistry, The University of Rome, Città Universitaria, 00185 Rome, Italy

J. P. Toennies
Max-Planck-Institut für Strömungsforschung, Bunsenstrasse 10, D-37073 Göttingen, Germany

(Received 12 July 1999; accepted 1 November 1999)

Diffusion Monte Carlo (DMC) calculations of the intermolecular vibrational ground states of $CO(He)_n$ clusters with $n=1-12$, for CO $v=0$ are reported. The intermolecular degrees of freedom of the clusters are treated in full dimensionality and a pairwise additive potential surface is used in which the He–CO interaction is described by a recently developed scheme which combines density functional theory (DFT) with the long-range dispersion contributions obtained from a perturbative theory. The calculations yield intermolecular ground-state energies, He density distributions, radial and angular density probability distributions. Optimal structures by SIMPLEX minimization have been calculated to estimate zero-point energy (ZPE) and quantum effects. © *2000 American Institute of Physics.* [S0021-9606(00)50105-6]

I. INTRODUCTION

Quantum clusters of helium present an opportunity to study both liquid clusters and highly quantum finite-size systems showing some very interesting peculiarities which make them unique in several respects. First, due to the very weak interactions between helium atoms, these clusters are by far the most weakly bound. In fact, it is only very recently that the existence of the H_2 molecule, with its single bound state, was confirmed by both mass spectrometry[1] and a novel diffraction method.[2] Second, the larger clusters provide a unique opportunity for studying the behavior of finite quantum systems. Third, the issue of superfluidity in finite clusters of helium is also of great interest. As a result, there has been considerable theoretical[3–6] and experimental[7–11] effort given to such clusters, which are known to remain liquid and are predicted to show superfluidity behavior at $T \leqslant 1.9$ K.[5,6] A potentially powerful method for detecting superfluidity in these systems[10,11] involves spectroscopic studies of atoms or molecules that act as dopant of the clusters.[8,12–16] When combined with the relevant theoretical work,[17–19] it is now clear that molecular probes can be used fruitfully to explore the local microscopic environment within the cluster.

Furthermore, van der Waals (vdW) heteroclusters $M(Rg)_n$, consisting of n rare-gas atoms Rg bound to a molecule M, have emerged in recent years among the most important finite-size prototype systems for studying solute–solvent interactions on a microscopic level.[16,20–24] $M(Rg)_n$ clusters are small enough to allow application of high-resolution laser spectroscopic techniques and supersonic molecular beams, usually reserved for isolated small molecules, to fundamental aspects of solvation in condensed matter. By gradually increasing the number of rare-gas atoms in the heterocluster, one has the unique opportunity to measure (as well as to simulate) the size dependence of structural, spectroscopic, and dynamical properties as they change from the behavior of small molecules to that characteristic of bulk phases. Electronic and infrared (IR) spectroscopy of molecules in size-selected rare-gas clusters have revealed that microsolvation leads to spectral shift of the absorption or emission bands, and to changes in the bandwidths and band shapes, all of which show strong and nonmonotonic dependence on the solvent cluster size.[16,20,21,23]

Theoretical analysis of probe species in helium clusters is still relatively sparse. Approximate calculations of the very small clusters $X(He)_n$, $N \leqslant 10$ have been made,[25,26] and recently variational and Green's function Monte Carlo methods have been applied to the $Cl_2(He)_2$ and $Cl_2(He)_3$ species.[27] Analysis of the high-resolution spectroscopy of such small clusters, e.g., $Cl_2(He)_n$ shows that even these very small species cannot be described by standard, rigid-rotor-based expansions, despite the presence of a strongly binding molecule which might be expected to increase the localization of the helium atoms.

The first theoretical study of a molecule attached to a helium cluster employed variational Monte Carlo computations on $H_2(He)_n$.[28] In this case, the interaction of the foreign species with He is very much like that of helium interacting with itself. The H_2–He potential is nearly isotropic and possesses a well depth only 2 K lower than that of the He–He potential. Successive studies were devoted to the

a)Author to whom correspondence should be addressed; electronic mail: fagiant@caspur.it

analysis of $SF_6(He)_n$[29] and $HF(He)_n$[30] clusters using the diffusion Monte Carlo (DMC) method to calculate ground-state energetics, structural properties, and the solvent-induced spectral shift of the vibrations of the dopant molecule.

The focus of this paper is to accurately characterize for the first time the vibrational ground states of various $CO(He)_n$ clusters, with n from 1 to 12, employing the diffusion Monte Carlo method. In our treatment, no approximation is made on the quantum dynamics of all internal degrees of freedom of these vdW clusters. We determine what are essentially the numerically exact ground-state energies of $CO(He)_n$ for potentials which are superpositions of CO–He and He–He interactions. In addition, the ground state wave functions of these clusters are analyzed in terms of probability distributions of the internal coordinates, all of which indicate highly delocalized motion of the surrounding He atoms.

In Sec. II we describe a recently developed treatment which combines density functional theory (DFT)[31] with the long-range dispersion interaction, obtained from perturbation theory, for the calculation of the full potential energy surface (PES) of CO–He system. In Sec. III we briefly explain the computational method employed to provide an accurate solution of the many-body Schrödinger equation, while we discuss the results of our calculations in Sec. IV.

II. THE CO–HE INTERACTION POTENTIAL

Because of its fundamental role in theoretical and experimental studies of the thermal balance in dense interstellar molecular clouds, the CO–He interaction has been the subject of many *ab initio* calculations. We will therefore try to briefly summarize below the results from such calculations and then we will discuss our present DFT+dispersion approach.

A. An outline of previous results

The earliest attempt was an evaluation of the rigid-rotor surface with the CO internuclear distance kept at its experimental value and with free-electron-gas methods employed to take correlation forces into account.[32]

Later *ab initio* calculations[33] considered an extended configuration interaction (CI) expansion, which however did not include the possible consequences of basis set superposition error (BSSE), and provided an entirely different PES. Further modifications on the CI interaction were suggested by a series of calculations, classical and quantum, of the transport properties.[34,35] An entirely different, empirical potential surface was then proposed, involving a new set of parameters obtained from the fully resolved infrared spectra of the vdW complex.[36] Finally, by using a model exchange-correlation treatment (XC) in the calculation and by guiding its optimization with infrared spectra, a more general empirical potential was recently suggested.[37]

Several *ab initio* calculations have also been completed in recent years. The rigid-rotor PES, in fact, has been computed using fourth-order Møeller–Plesset (MP) perturbation theory,[38] while a similar approach was employed in another recent publication[39] where the MP fourth-order treatment was carried out and the rotovibrational energy levels of the complex were evaluated with the collocation method. Both the above calculations have included the effects of the BSSE correction. A further comparison with the same infrared spectra has been carried out again more recently starting from a theoretical calculation which used symmetry-adapted perturbation theory (SAPT).[40]

B. The DFT calculations

The use of density functionals theory[31] for the treatment of either hydrogen-bonded or van der Waals systems has been much less widespread than the study of thermochemical data or molecular equilibrium geometries.[41] On the other hand, because of the computational difficulties present in the evaluation of such weak forces, the path to some reliable DFT method which can be employed to test dynamic observables for such systems seems a very tempting one to follow.

It therefore becomes interesting to explore the applicability of any DFT method to the broad range of configurations sampled by the intermolecular interactions in order to extend the possible use of *ab initio* methods to increasingly more complicated multielectron partners. One knows, in fact, that the inclusion of the all-important electron correlation effects occurs rather directly within DFT methods while it happens only slowly within CI expansions, where necessary truncations can often jeopardize the whole reliability of the final results.

One can begin by writing the familiar expression for the total energy[42,43]

$$E_{\mathrm{tot}}=E[\rho]=\sum_i \epsilon_i-\frac{1}{2}\int \frac{\rho(\mathbf{r})\rho(\mathbf{r}')}{|\mathbf{r}-\mathbf{r}'|}d\mathbf{r}\,d\mathbf{r}'+E_{\mathrm{xc}}[\rho]-\int V_{\mathrm{xc}}\rho(\mathbf{r})d\mathbf{r}, \tag{1}$$

where

$$\sum_i^N \epsilon_i=T_s[\rho]+\int V_{\mathrm{eff}}(\mathbf{r})\rho(\mathbf{r})d\mathbf{r}, \tag{2}$$

and

$$V_{\mathrm{eff}}(\mathbf{r})=V(\mathbf{r})+\int \frac{\rho(\mathbf{r}')}{|\mathbf{r}-\mathbf{r}'|}d\mathbf{r}'+V_{\mathrm{xc}}(\mathbf{r}), \tag{3}$$

where $V(\mathbf{r})$ is the potential energy between nuclei and electrons and $V_{\mathrm{xc}}(\mathbf{r})$ is the exchange-correlation potential energy. The above result is exact provided we know the kinetic energy functional form in Eq. (2) and the E_{xc} functional form in Eq. (1).[42] It is toward the solution of this specific aspect that many computational and theoretical efforts have been directed in recent years.[41,42,44] Here, T_s is the sum of single-particle kinetic energy operators and E_{xc} is the nonclassical exchange and correlation energy contributions coming from the chosen form of the functional of the total electronic density $\rho(\mathbf{r})$ in the ground electronic state of the system.

Among the many possible forms of the E_{xc} contribution discussed at length by the relevant DFT literature,[41–44] the adiabatic connection methods (ACM)[45–49] have recently be-

come popular for calculating molecular electronic properties. The starting point of these approaches is the adiabatic connection formula[50,51]

$$E_{xc}=\int_0^1 U_{xc}^{\lambda}\,d\lambda, \tag{4}$$

where λ is an interelectronic coupling-strength parameter that ''switches on'' the Coulomb repulsion between electrons and U_{xc}^{λ} is the potential energy of exchange correlation at an intermediate coupling strength λ.

This formula ''connects'' the noninteracting Kohn–Sham reference system ($\lambda=0$) to the fully interacting system ($\lambda=1$) through a continuum of partially interacting systems ($0\leqslant\lambda\leqslant1$), all of which have the same density ρ (i.e., the density of the real system). It has been shown in the literature[45] that the simplest approximation to Eq. (4) can be expressed by a two-point formula

$$E_{xc}\simeq\tfrac{1}{2}E_{xc}^{\lambda=0}+\tfrac{1}{2}E_{xc}^{\lambda=1}. \tag{5}$$

An application of Eq. (5) is the so-called half–half approximation[45]

$$E_{xc}\simeq\tfrac{1}{2}E_x+\tfrac{1}{2}E_{xc}^{\mathrm{LSDA}}, \tag{6}$$

where the E_{xc}^{LSDA} contribution is calculated following the local spin density approximation (LSDA) in which the exchange part is given by the formula proposed by Slater[52] and the correlation part is derived from the formula described by Vosko, Wilk, and Nusair,[53] while the E_x contribution is the pure exchange energy of the Kohn–Sham (KS) orbitals from a single determinant.[45]

The full calculation of the anisotropic interaction was therefore carried out by fixing, at first, the r_{CO} distance at 2.1323 a_0 (equilibrium bond distance) and by evaluating different orientations between $\theta=0°$ and $\theta=180°$. To introduce the vibrational dependence of CO, the same type of calculation has been repeated for six other values of r_{CO} in order to include the first five diatomic vibrational states. In all the calculations of the present work the $\theta=0°$ orientation corresponds to the collinear He–C–O structure.

The quality of the Gaussian basis set expansion employed was of the quadruple-zeta (cc-pVQZ) level,[54] where the original and contracted sets of functions were, respectively: $(7s,3p,2d,1f)$ and $[4s,3p,2d,1f]$ on the He atom, $(12s,6p,3d,2f,1g)$ and $[5s,4p,3d,2f,1g]$ on the C atom, and $(12s,6p,3d,2f,1g)$ and $[5s,4p,3d,2f,1g]$ on the oxygen atom.

One important aspect of the full evaluation of the weak, vdW type of PES involves the inclusion of long-range (LR) dispersion contributions

$$V_{\mathrm{DISP}}(r,R,\theta)=-\frac{C_6(r,\theta)}{R^6}-\frac{C_7(r,\theta)}{R^7}-\frac{C_8(r,\theta)}{R^8}, \tag{7}$$

where the coefficients and their θ-dependence, as well as the dependence on r_{CO}, have often been discussed in the literature.[55]

There are many ways in which the LR dispersion tail can be smoothly joined onto the short-range DFT interaction. However, because of the difference in anisotropy of the two types of interaction, the resulting PES will be mostly affected in the well region. Since the present potential is expanded into Legendre polynomials

$$V(r,R,\theta)=\sum_{\lambda} V_{\lambda}(r,R)P_{\lambda}(\cos\theta), \tag{8}$$

one could assume that the DFT short-range region already contains, for each of the coefficients, the correct coulomb, exchange, and correlation energy contributions as given within the prescription of Eq. (1). Hence, one can subtract the first two contributions from the half–half (HH) calculations for each of the multipolar coefficients of Eq. (8)[56] by carrying out additional separate HF calculations with the same basis set discussed before and which is being employed to obtain the KS orbitals within the self-consistent field (SCF) part of the full HH interaction. One can therefore write

$$V_{\lambda}^{\mathrm{DFT}}(r,R)=V_{\lambda}^{\mathrm{HH}}(r,R)\simeq V_{\lambda}^{\mathrm{HF}}(r,R)+V_{\lambda}^{\mathrm{corr}}(r,R), \tag{9}$$

from which

$$V_{\lambda}^{\mathrm{HH}}(r,R)-V_{\lambda}^{\mathrm{HF}}(r,R)\simeq V_{\lambda}^{\mathrm{corr}}(r,R). \tag{10}$$

If one further presumes that at least the behavior of short-range correlation forces is given realistically by the DFT calculations, then one could modify the perturbative dispersion terms of Eq. (7) by using the values from Eq. (10) to scale them as they come closer in from the long-range region. One should also remember here that, as is known, no long-range dispersion contributions are included in a DFT model at large distances.[42] Hence, the long-range (LR) contributions could be rewritten using Eqs. (7) and (10) as

$$V_{\lambda}^{\mathrm{LR}}(r,R)=V_{\lambda}^{\mathrm{DISP}}(r,R)+D_{\lambda}V_{\lambda}^{\mathrm{corr}}(r,R). \tag{11}$$

Each final multipolar coefficient can therefore be obtained by matching the two regions at the points where, for each Legendre component, the logarithmic derivatives of the dispersion and correlation branches are equal, a requirement that produces the D_{λ} scaling factors which correct the $V_{\lambda}^{\mathrm{DISP}}$ radial dependence around the well region and makes the potential continuous in that region, in analogy to what was attempted earlier by Parker and Pack[56] in other vdW systems

$$V_{\lambda}(r,R)=\begin{cases} V_{\lambda}^{\mathrm{DFT}}(r,R) & \text{for } R<R_{\lambda} \\ V_{\lambda}^{\mathrm{HF}}(r,R)+V_{\lambda}^{\mathrm{LR}}(r,R) & \text{for } R>R_{\lambda} \end{cases}. \tag{12}$$

Having defined in the above way the dispersion contributions, we obtained a modified DFT surfaces for the He–CO system which we shall call the half–half with scaled dispersion (HHSD). The results from such calculations have already been discussed in detail considering the equilibrium bond distance for the CO molecule ($r=2.1323a_0$) either for the He–CO[57] or Ar–CO[58] systems. Here, we report in Fig. 1 the comparison, at fixed orientations, between the HHSD potential and the best two potentials known in literature: the semiempirical XC of Ref. 37 and the *ab initio* SAPT of Ref. 40. The plots refer to the rigid-rotor surface with the C–O distance fixed to the experimental equilibrium value of 2.1323 a_0. In the upper panels we show the repulsive region and in the lower panels the well region. It is possible to see

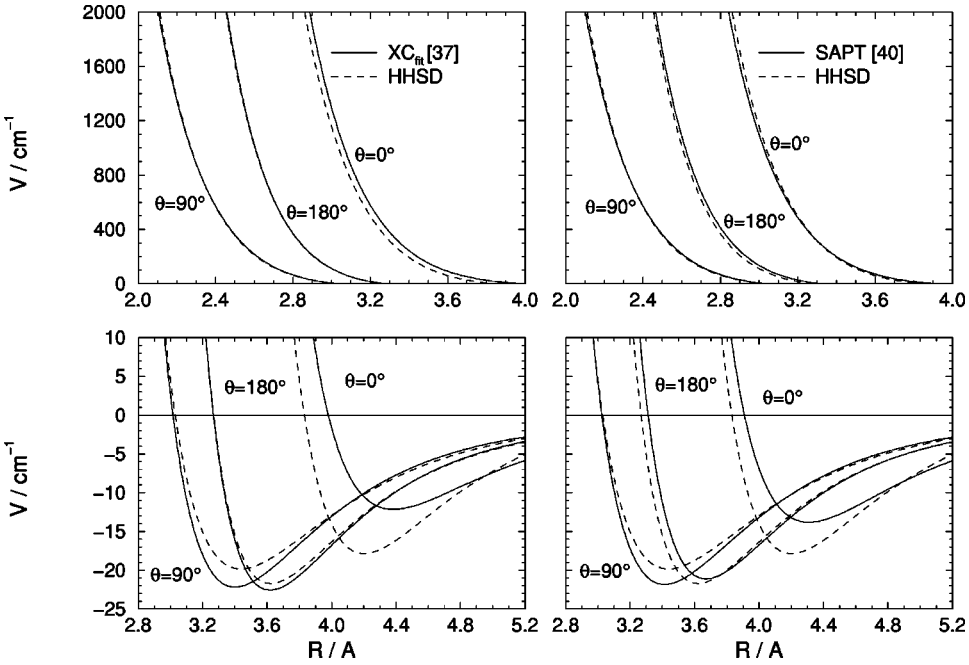

FIG. 1. Comparison of the repulsive regions (top) and of the well regions (bottom) for different orientations of the present DFT potential (HHSD) with respect to the last semiempirical surface (XC of Ref. 37) and the last computed *ab initio* PES (SAPT of Ref. 40).

that the HHSD potential follows closely the best available potential functions in the short-range region, although it still shows a slightly less anisotropic behavior that produces in turn a more pronounced minimum for the $\theta=0°$ orientation. On the whole, however it gives us a very realistic representation of the best available PES for the present system.

The potential has been described by 13 multipolar coefficients and their properties have been discussed in detail in our previous work.[57] The actual radial coefficients are available upon request to the corresponding author of the present work.

III. THE STOCHASTIC MODEL

The diffusion Monte Carlo (DMC) method[59] has been extensively discussed in a number of papers.[60–63] We therefore refer the reader to that literature for a fuller discussion, while this section merely summarizes the main features of the method, our particular implementation, and some specific extensions developed for the present application.

The key idea of the DMC method is the isomorphism between the time-dependent many-body Schrödinger equation and a multidimensional reaction-diffusion equation with anisotropic diffusion coefficients. Introduction of imaginary time $\tau=it/\hbar$, shifting of the absolute energy scale by a quantity E_{ref}, and identification of the inverse mass terms with diffusion coefficients D_j and of the shifted potential $[V(\mathbf{r})-E_{\mathrm{ref}}]$ with position-dependent rate terms $k(\mathbf{r})$ leads to the following equations which show this analogy:

$$i\hbar\frac{\partial\Psi(\mathbf{r},t)}{\partial t}=-\sum_j\frac{\hbar^2}{2m_j}\nabla_j^2\Psi(\mathbf{r},t)+[V(\mathbf{r})-E_{\mathrm{ref}}]\Psi(\mathbf{r},t), \tag{13}$$

$$\frac{\partial\Psi(\mathbf{r},\tau)}{\partial\tau}=-\sum_j\frac{\hbar^2}{2m_j}\nabla_j^2\Psi(\mathbf{r},\tau)+[V(\mathbf{r})-E_{\mathrm{ref}}]\Psi(\mathbf{r},\tau), \tag{14}$$

$$\frac{\partial C(\mathbf{r},t)}{\partial t}=-\sum_j D_j\nabla_j^2C(\mathbf{r},t)+k(\mathbf{r})C(\mathbf{r},t). \tag{15}$$

Knowledge of the structure of the wave function can be fruitfully exploited for increased accuracy by introducing a guiding function Ψ_T that is meant to approximate the true wave function. A common ansatz for atomic clusters and bulk systems[64] expresses Ψ_T as a product over a set of one-dimensional functions Φ defined over all pairs of particles

$$\Psi_T(\mathbf{R},\mathbf{p})=\prod_{i<j}\Phi_{ij}(R_{ij};\mathbf{p}), \tag{16}$$

where R_{ij} is the distance between particles i and j, and $\mathbf{p}$ denotes the set of adjustable parameters controlling the trial wave function. Following Ref. 39, we write Ψ_T as a product over pairwise radial function Φ connecting the rare-gas atoms and a product over two-dimensional functions χ describing the anisotropic CO–He contribution:

$$\Psi_T(\mathbf{R};\mathbf{p})=\prod_{i\in\mathrm{He}}\chi_i(R_i,\theta_i;\mathbf{p})\times\prod_{i<j\in\mathrm{He}}\Phi_{ij}(R_{ij};\mathbf{p}). \tag{17}$$

The R_{ij} are the distances between rare-gas atoms i and j, and R_i, θ_i are the Jacobi coordinates describing the distance between rare-gas atom i and the center of mass of CO and the angle between the R_i vector and the CO bond vector. This form of Ψ_T satisfies the proper exchange symmetry for ^{4}He. There is no explicit dependence of Ψ_T on the CO distance since our current treatment assumes adiabatic separability between the molecular vibration and the intermolecular vibrations in agreement with previous treatments of small van der Waals complexes.[65]

To avoid unnecessary lengthening of the present paper, we will discuss elsewhere the vibrational dependence of the interaction and the shift of the CO vibrational frequency induced by the surrounding clusters of helium atoms.[66] Previous experience with pure[29] and mixed[30] helium clusters

showed that Jastrow functions are a good choice for Φ and were also employed in the present work. In particular, we used the isotropic part of the best trial wave function obtained from a previous variational Monte Carlo (VMC) calculation. For the part concerning the interaction CO–He we used a constant function instead.

The introduction of Ψ_T results in additional drift terms in the diffusion equation which direct the random walkers into regions where the trial wave function is large. At the same time, the rate terms are now controlled by the local energy defined as

$$E_{\text{local}}(\mathbf{r}) = \Psi_T^{-1}(\mathbf{r})\hat{H}\Psi_T(\mathbf{r}) = \Psi_T^{-1}(\mathbf{r})\hat{T}\Psi_T(\mathbf{r}) + V(\mathbf{r}), \tag{18}$$

which is a smoother function of the coordinates than the potential and reduces the variance of the energy estimators

$$\frac{\partial(\Psi\Psi_T)}{\partial\tau} = \left[\sum_j \frac{1}{2m_j}\nabla_j^2(\Psi\Psi_T) - \frac{1}{m_j}\nabla_j(\Psi\Psi_T\nabla\ln\Psi_T)\right] - [\Psi_T^{-1}T\Psi_T + V(\mathbf{r}) - E_{\text{ref}}](\Psi\Psi_T). \tag{19}$$

A random walk technique is used to calculate the steady-state solution of the diffusion equation corresponding to a given quantum problem. A large ensemble of random walkers is propagated with time steps $\Delta\tau$ starting from some arbitrary initial distribution. The propagation from τ to $\tau+\Delta\tau$ consists of random Gaussian displacements of the Cartesian coordinates and systematic moves under the influence of the quantum drift force $F(\mathbf{r}) = \Psi_T\nabla\ln\Psi_T$ and an update of a weight carried by each random walker. Additionally we use a Metropolis type acceptance check for each attempted move[62] such that for arbitrary time steps the number density of walkers is given by Ψ_T^2, while their weights are a stochastic sample of the local value of Ψ/Ψ_T. This has been shown to result in large reductions of the time-step error of DMC calculations. Our implementation uses a global check after trial moves have been made for all particles. The short time approximation to the Green's function appropriate for Eq. (19) is

$$G(\mathbf{r}\to\mathbf{r}';\Delta\tau) = \prod_j \left[\left(\frac{m_j}{2\pi\Delta\tau}\right)^{3/2} \times\exp\left\{-\frac{m_j}{2\Delta\tau}\left(\mathbf{r}_j - \mathbf{r}'_j - \frac{\Delta\tau}{2m_j}\mathbf{F}_j(\mathbf{r})\right)^2\right\}\right] \times\exp\left\{-\Delta\tau_{\text{eff}}\left(\frac{E_{\text{local}}(\mathbf{r})+E_{\text{local}}(\mathbf{r}')}{2} - E_{\text{ref}}\right)\right\}. \tag{20}$$

The modified time step $\Delta\tau_{\text{eff}}$ appears in the growth term of Eq. (20) because not all moves attempted according to $G(\mathbf{r}\to\mathbf{r}';\Delta\tau)$ are accepted in the Metropolis step. Proposed moves from $\mathbf{r}$ to $\mathbf{r}'$ are carried out with probability

$$P(\mathbf{r}\to\mathbf{r}') = \min\{1, A(\mathbf{r}\to\mathbf{r}')\}, \tag{21}$$

$$A(\mathbf{r}\to\mathbf{r}') = \frac{|\Psi_T(\mathbf{r}')|^2 G(\mathbf{r}'\to\mathbf{r})}{|\Psi_T(\mathbf{r})|^2 G(\mathbf{r}\to\mathbf{r}')}. \tag{22}$$

The asymmetric transfer function $G(\mathbf{r}\to\mathbf{r}';\Delta\tau)$ has to be explicitly taken into account in this acceptance decision. Therefore, the effective time step $\Delta\tau_{\text{eff}}$ is defined through the ratio of accepted displacements and attempted displacements according to

$$\Delta\tau_{\text{eff}} = \Delta\tau\frac{\langle\Delta\mathbf{r}^2\rangle_{\text{acc}}}{\langle\Delta\mathbf{r}^2\rangle_{\text{att}}}. \tag{23}$$

As mentioned before, our specific implementation assigns a variable weight to each random walker. As a consequence of the exponential weight update, the sum of weights $W(\tau) = \Sigma_i w_i(\tau)$ grows or decays according to the mismatch between E_{ref} and the average local energy.

Walkers whose relative weight $w_{\text{rel}} = w_i/W(\tau)$ falls below a preselected value $w_{\min}$ are eliminated randomly from the ensemble with probability $p_- = 1 - w_{\text{rel}}$ or retained and assigned the average weight $W(\tau)/n_{\text{walk}}$ with probability $p_+ = w_{\text{rel}}$. Walkers whose relative weight grows beyond a maximum value $w_{\max}$ are split into $n_w = \text{int}(w_{\text{rel}}+u)$ walkers of weight w_i/n_w, where u is a uniform random number. The values of $w_{\min}$ and $w_{\max}$ are chosen such that the average number of walkers remains approximately constant during the run, while the instantaneous ensemble fluctuates. These mechanisms ensure that the walkers remain concentrated in relevant regions of configuration space without introducing artificial sources or sinks and can be easily generalized to a situation with correlated walks on several surfaces.

After equilibration of the initial random walker distribution, the ensemble average of E_{local}, which will be referred to as E_{mean} in this paper, is identical with the ground-state energy irrespective of Ψ_T and is only subject to statistical fluctuations. The ground-state energy can also be computed from the rate at which the total weight of the ensemble grows or decays as τ elapses. This estimator is called the growth energy

$$E_{\text{growth}} = E_{\text{ref}} - \frac{\partial\ln W(\tau)}{\partial\tau}, \tag{24}$$

and, depending on the system being considered, is known at times to have a smaller time-step dependence than E_{mean}.[63] Both energy estimators were always extremely close to each other in our simulations, the difference never exceeding half the standard deviation of energies. We therefore report only our values for E_{mean} as E_0 values.

In order to take into account the slow decay of the weak He–He interaction terms as the distances increased, we have employed extended temporal runs that ensure the correct sampling of the full PES by the random walkers.

A. Calculation of expectation values

Arbitrary property expectation values $\langle\hat{A}\rangle$ are computed by replacing integrals by sums over samples

$$\langle\hat{A}\rangle = \frac{\int\Psi^*(\mathbf{x})\hat{A}\Psi(\mathbf{x})d\mathbf{x}}{\int|\Psi(\mathbf{x})|^2 d\mathbf{x}}, \tag{25}$$

$$\approx \frac{1}{N}\sum_{i=1}^{N}\Psi^{-1}(\mathbf{x})\hat{A}\Psi(\mathbf{x}), \tag{26}$$

where **x**'s indicate some general coordinates and the correct $|\Psi|^2$ quantity is obtained from the estimated, trial Ψ_T values by using the technique of descendant weighting.[64] Only expectation values of local operators are directly accessible with the DMC scheme. In this case, the integration reduces to an average over operator values $A(\mathbf{x})$

$$\langle \hat{A} \rangle \approx \frac{\Sigma_i^N w_i A(\mathbf{x}_i)}{\Sigma_i^N w_i}. \tag{27}$$

This technique is in particular applicable to the positional correlation functions which are very useful in visualizing the structure of the clusters. The radial distribution of rare-gas atoms relative to the center of mass of the whole cluster is computed as

$$P_{\mathrm{rad}}(R) = \frac{1}{n} \sum_i^n \left\langle \frac{\delta(R_i - R)}{R^2} \right\rangle_{\mathrm{walk}}. \tag{28}$$

The radial distribution function can be easily converted to the spherically averaged radial rare-gas density distribution $\rho(R)$

$$\rho(R) = \frac{n}{4\pi} P_{\mathrm{rad}}(R). \tag{29}$$

In a similar way, we compute two-dimensional histograms in cylinder coordinates to analyze the density distribution $\rho(r,z)$ of helium atoms around the CO molecule. The CO bond is chosen at the z axis and the perpendicular distance of helium atoms to this axis defines the polar radius r. The origin coincides with the center of mass (CM) of CO and the carbon atom is on the positive z axis. The density distribution is computed as

$$\rho(r,z) = \frac{n}{2\pi} \sum_i \left\langle \frac{\delta(r_i - r)}{r} \delta(z_i - z) \right\rangle_{\mathrm{walk}}, \tag{30}$$

$$n = 2\pi \int_0^\infty \int_{-\infty}^\infty \rho(r,z) r \, dr \, dz. \tag{31}$$

This quantity is accumulated on a grid which is equidistant in z and r^2 which eliminates the need to take square roots during the data collection.

B. The global potential energy function

All calculations were done with a purely pairwise additive potential energy surface based on the DFT *ab initio* part for the He–CO interaction and the empirical HFD-B potential for He.[67] For the He–CO interaction, we used the adiabatic expression

$$V_{v=0}^{\mathrm{HeCO}}(R,\theta) = \langle V^{\mathrm{HeCO}}(R,\theta,r_{\mathrm{CO}}) \rangle_{v=0} = V_{00}(R,\theta), \tag{32}$$

where the index $v=0$ indicates averaging over the CO ground-state wave function obtained by solving the Schrödinger equation for the diatomic potential of Ref. 68. Within this approximation, the adiabatic potential of the $CO(He)_n$ cluster is now expressed as

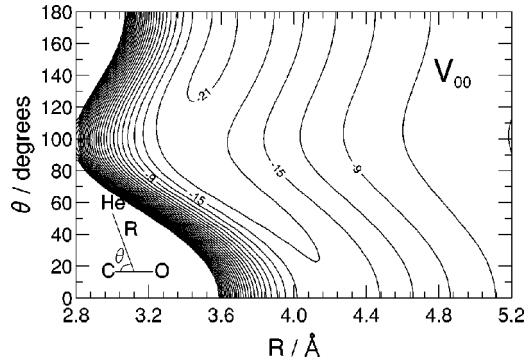

FIG. 2. Energy levels of the potential energy surface for the adiabatic V_{00} potential discussed in the main text. The energy levels are in units of cm^{-1}.

$$V_{\mathrm{total}} = \sum_{i=1}^n V_{v=0}^{\mathrm{HeCO}}(R_i, \theta_i) + \sum_{i<j}^n V^{\mathrm{HeHe}}(R_{ij}), \tag{33}$$

where R_{ij} are distances between rare-gas atoms i and j, and R_i, θ_i are Jacobi coordinates describing the distance between rare-gas atom i and the center of mass of CO and the angle between the r_i vector and the CO bond vector. Although many-body forces are included in each term of the first sum on the right-hand side of (33), no three-body or higher-order forces are added to it or to the second sum on the right-hand side of Eq. (33). We shall comment further on this point when discussing the results from the present work.

In Fig. 2 we show the adiabatic potential energy contours in (R,θ) coordinates, where one clearly sees that our calculations confirm the presence of only one minimum close to the linear configuration C–O–He and the existence of a weak angular anisotropy as discussed in Ref. 57.

IV. DISCUSSION OF RESULTS

In this section we will discuss in detail the ground-state energetics and structural properties of the $CO(He)_n$ clusters, while the discussion of the other important aspect of this study concerning the vibrational frequency shift caused by the cluster environment on the ''solute'' CO molecule will be reported in a following publication. We will also discuss there a comparison with the results obtained from the $CO(Ar)_n$ clusters[69] analysis with DMC methods.

A. Binding and evaporation energies

The adiabatic ground-state energies for $CO(He)_n$ when the CO molecule is in its vibrational state $v=0$, calculated from the DMC approach described in Sec. III, are shown in the left panel of Fig. 3 for clusters of different sizes. One clearly sees that the slope of the line is practically a constant when the number of helium atoms is increased. This fact becomes more evident when one looks at the single evaporation energy; that is, the energy necessary to evaporate one He atom from the cluster. This quantity, which is a measure of the relative stability of clusters of different sizes, is shown in the right panel of the same figure. As mentioned before, it is possible to note that there is no particular evidence of ''magic number,'' i.e., the clusters of different sizes all have

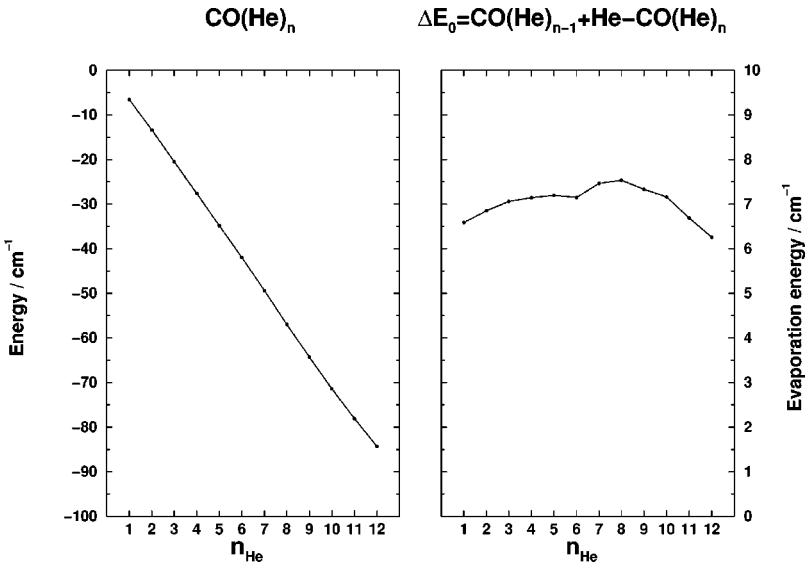

FIG. 3. Computed binding energies (left panel) and single-atom evaporation energies (right panel) from the DMC calculations, as a function of atom number in the $CO(He)_n$ clusters.

practically the same relative stability. This result is completely different from that obtained for the $CO(Ar)_n$ clusters, in which it was possible to observe more complicated energetics,[69] and can be clearly related here to the very characteristic behavior of the helium atoms when thought of as ''solvent'' atoms[29,30] as in the present process.

In Fig. 4 we report instead the 3D plot of the He density for some $CO(He)_n$ clusters, represented in cylindrical coordinates where the *z* axis corresponds to the C–O axis with the oxygen located at negative values and *r* corresponds to the radius of the cylinder. From these density distributions, one sees very clearly the floppiness of such clusters which correspond to diffuse distributions of the rare-gas atoms around the CO molecule which have larger probability of being located in the regions where the interaction is stronger. This is most evident in the CO(He) cluster, where our calculations show a diffuse distribution of the He atom associated to all the orientations around the bond axis of the diatomic. It reaches its maximum value in correspondence to the global minimum of the adiabatic potential surface, that is close to the linear configuration C–O–He. It is obviously more difficult to correspondingly locate the minimum of the multidimensional surface for the largest $CO(He)_n$ clusters, but it is clear from the plots of the global density that the distributions of the rare-gas atoms become more uniform around the CO with the increasing of the cluster size, hence providing a solvation shell for the diatomic impurity. This solvation can be further understood by comparing the relative strengths of He–He and He–CO interactions. These interactions, although very weak, are in fact different from each other. In particular, the attractive part between He atoms is weaker than that for the He–CO portion, and therefore the rare-gas atoms in the clusters are distributed as shown by the calculations in order to optimize their interactions with the diatomic molecule. Considering the different strengths of the pair interactions, it then becomes possible to explain the constant values for the evaporation energies: for these small clusters, in fact, the helium atoms are practically indistinguishable either by spatial position or by their energy. The obtained value of ~ 7 cm^{-1} roughly corresponds, therefore, to the binding energy of a single helium atom to the CO–He system, hence showing that for these small clusters the role of additional, surrounding He atoms is marginal.

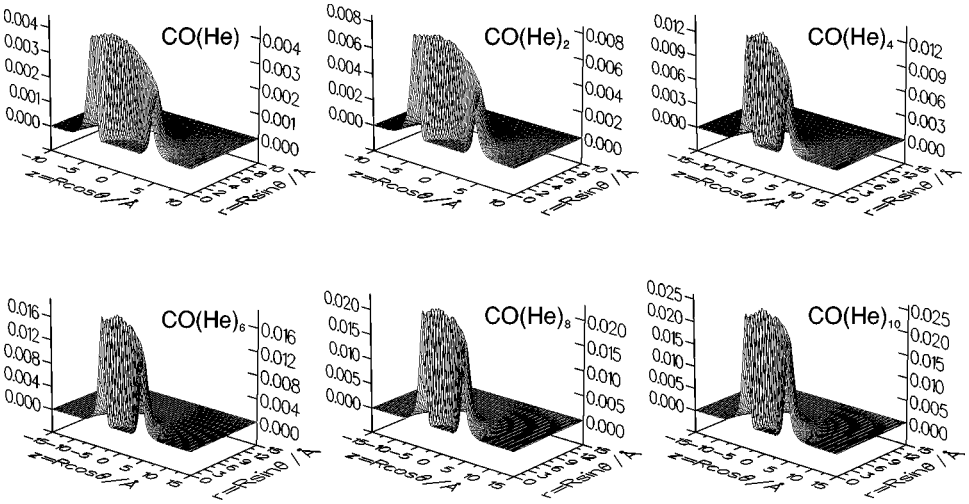

FIG. 4. 3D density distributions of He atoms around the CO molecule obtained from DMC calculations for clusters of different size. Distances in Å and densities in $Å^{-3}$.

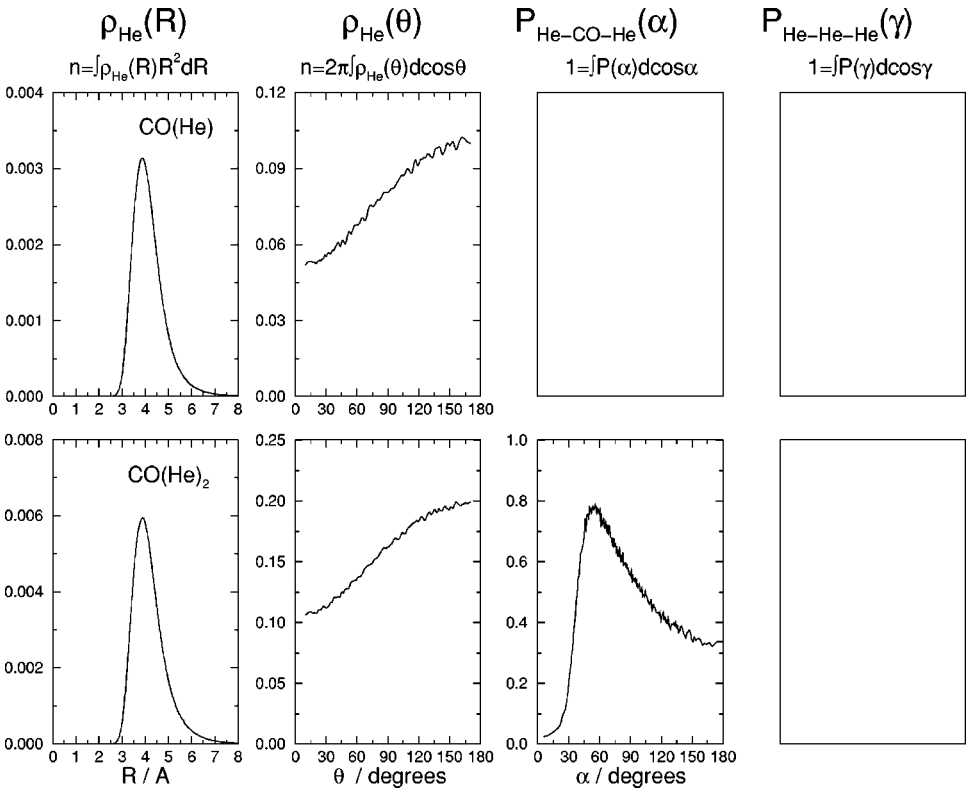

FIG. 5. Radial and angular density distributions for the $CO(He)_n$ clusters. Upper panels: for the $n=1$ case; lower panels: for the $n=2$ case. The panels represent, from left to right: radial distributions from the molecule center of mass; angular distributions for one Ar atom's Jacobi angle; angular distributions for two He atoms with respect to the molecular center of mass; angular distributions for three He atoms with respect to the middle atom of each trimer.

B. Radial and angular correlation values

In order to obtain more information about the structure of the present clusters, we have also analyzed the radial and the angular density distribution probability of the He atoms. In Figs. 5–10 we report in their first columns the radial density distribution and in the second the angular density distribution in which the θ angle corresponds to the angle between the bond axis and the vector from the center of mass of CO. The third and fourth columns further show the angular distribution probability in which the α angle is the angle between the center of mass of CO and two helium atoms and the γ angle is the angle between three He atoms.

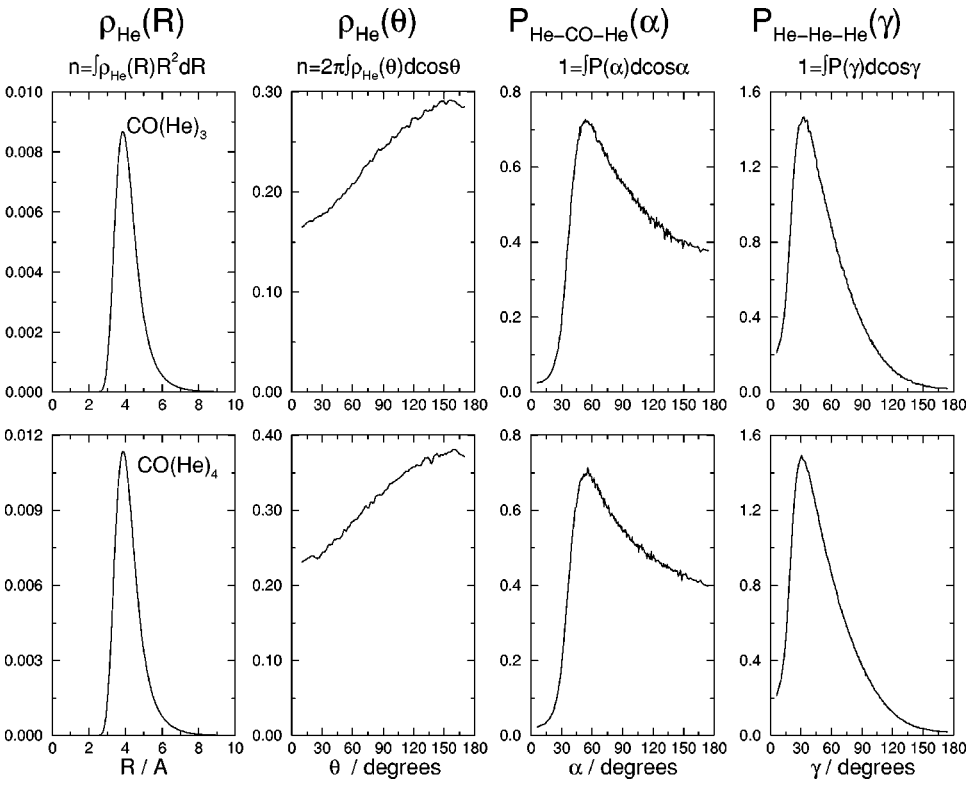

FIG. 6. Same as in Fig. 5 but for $n=3$ (upper panels) and $n=4$ (lower panels).

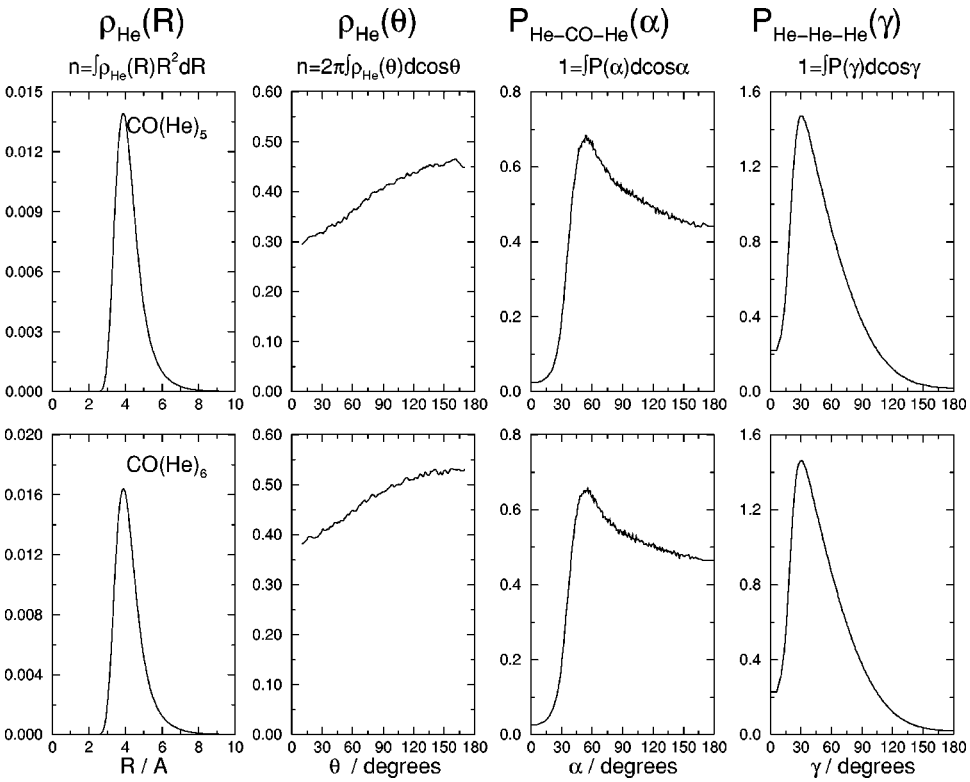

FIG. 7. Same as in Fig. 5 but for $n=5$ (upper panels) and $n=6$ (lower panels).

Looking at the first column, one clearly sees that the largest peak of the radial density is centered at about 4.0 Å, which corresponds to the region of the minimum for the He–CO interaction. It is also possible to note that, contrary to what happens in the case of $CO(Ar)_n$ clusters,[69] there is no appearance of outer peaks at larger distances: this is a further confirmation that all the helium atoms in these small clusters belong to the same solvation shell and are practically indistinguishable from each other. This suggestion is confirmed by the angular distributions: in the second column it is possible to see a very diffuse distribution of rare-gas atoms around the CO impurity, with an increasing probability to find He atoms at the oxygen side of diatomic (stronger attraction He–CO) as the cluster size is increased, while both

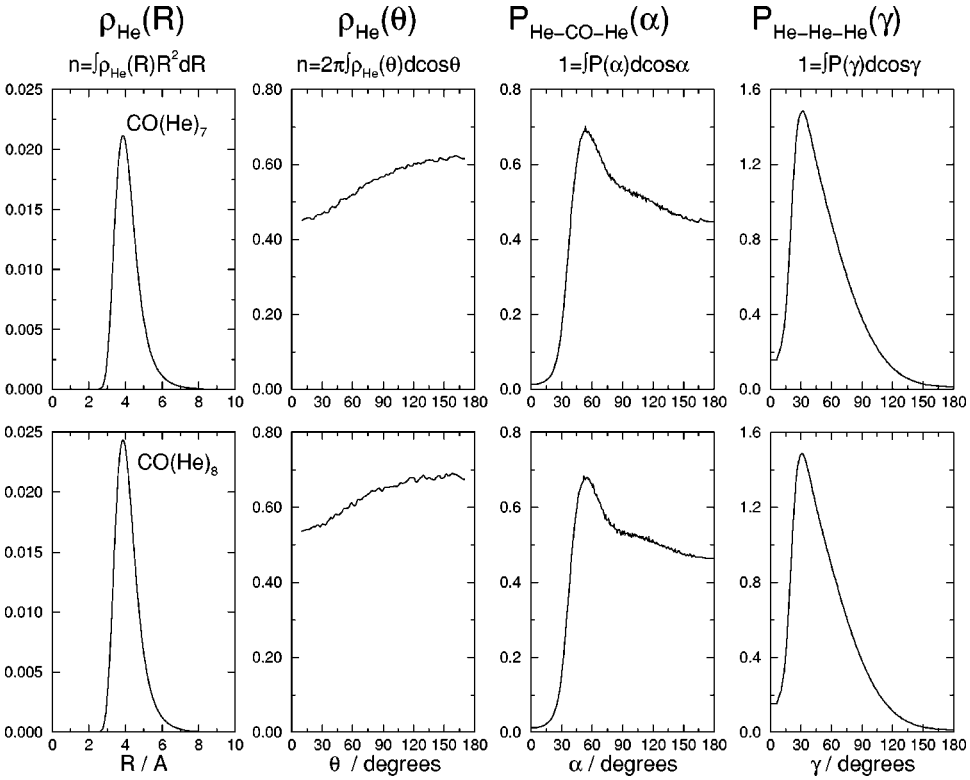

FIG. 8. Same as in Fig. 5 but for $n=7$ (upper panels) and $n=8$ (lower panels).

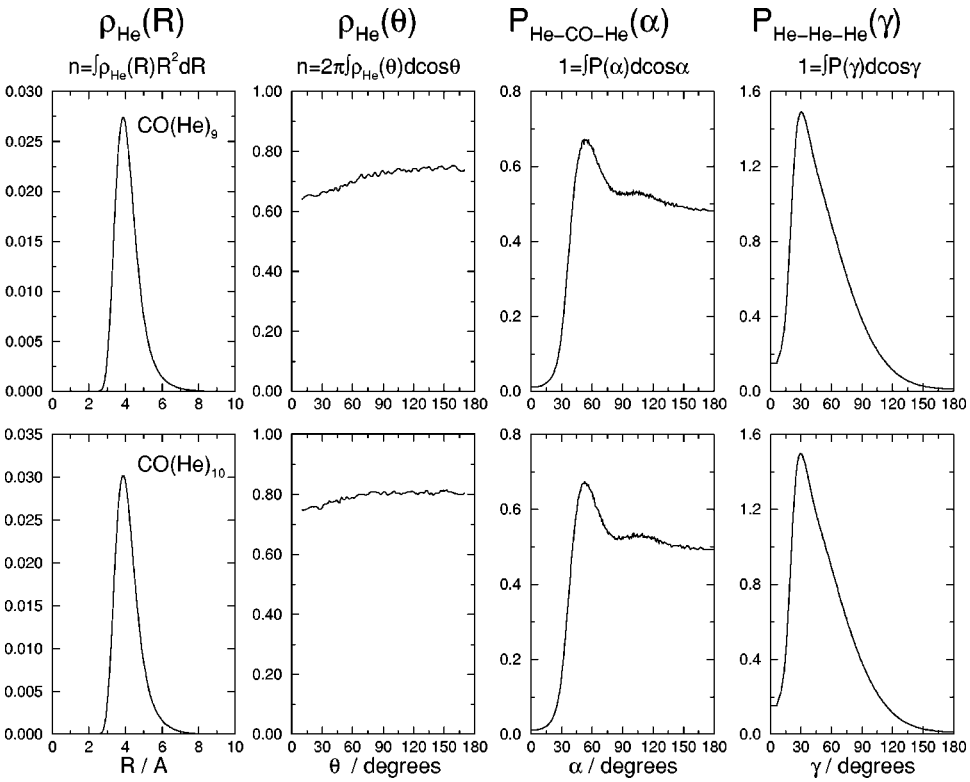

FIG. 9. Same as in Fig. 5 but for $n=9$ (upper panels) and $n=10$ (lower panels).

the probability distributions for the α and γ angles show very broadly spread out contours, contrary to what was observed for the $CO(Ar)_n$ clusters,[69] where we saw several narrow peaks which increased in number when the size of cluster was increased. The presence of peaks in the angular distributions is simply a consequence of the location of the attractive minima of the Rg–Rg interactions, where the repulsive walls prevent putting any two atoms closer than their R_{min} values. These results point to a very pronounced solvation effect of He atoms on the CO as a ''solute'' and further suggest that quantum effects are very important in the vdW clusters where several minima exist and in which directional bonding cannot be described in terms of the usual ''balls and sticks'' picture.

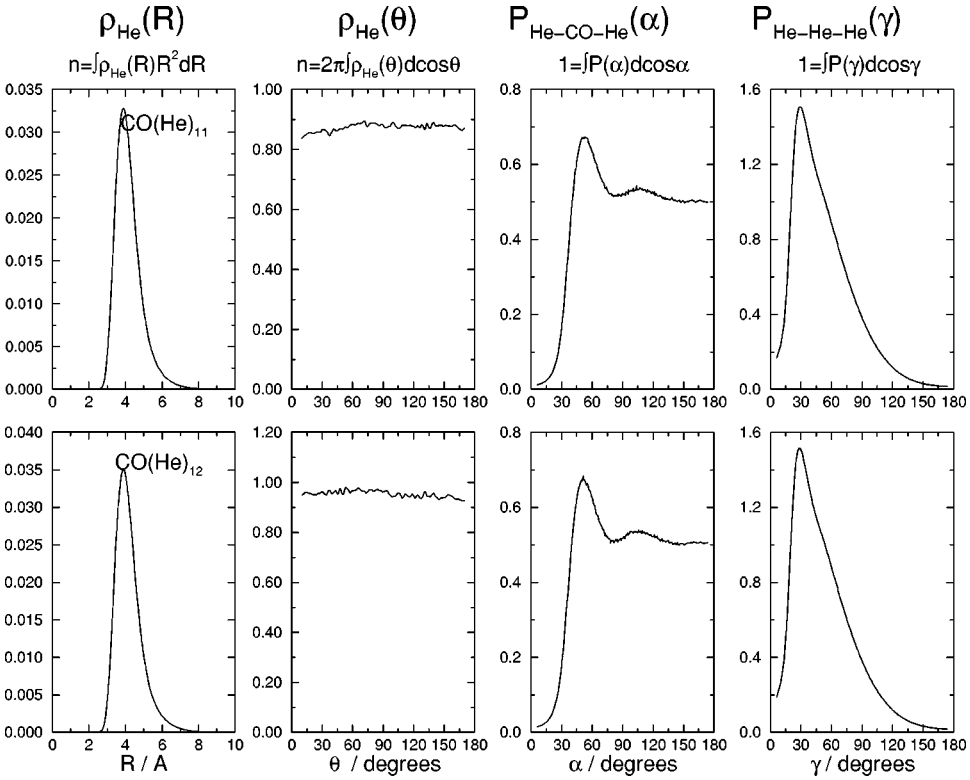

FIG. 10. Same as in Fig. 5 but for $n=11$ (upper panels) and $n=12$ (lower panels).

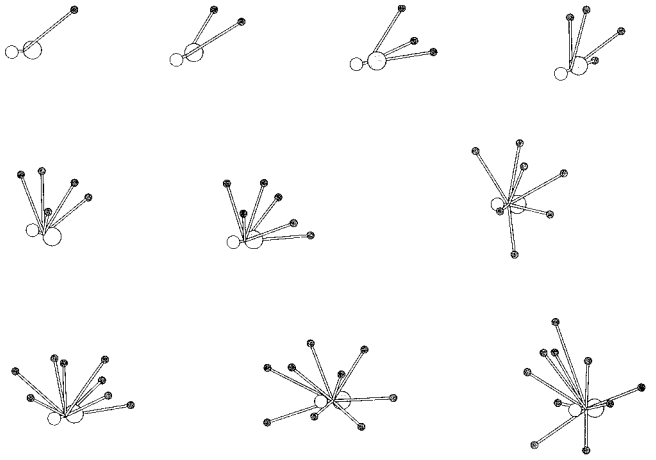

FIG. 11. SIMPLEX optimization structures for the $CO(He)_n$ clusters using the interactions described in the main text. First row, from left to right: the clusters with n from 1 to 4. Second row, from left to right: the clusters with n from 5 to 7. Third row, from left to right: the clusters with n from 8 to 10.

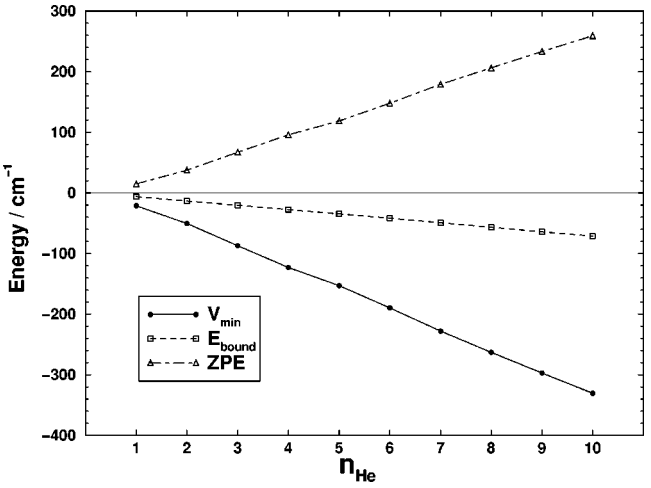

FIG. 12. Computed total energies as a function of cluster size (with n from 1 to 10). Solid line: from the SIMPLEX minimum structures; dashed line: from the DMC calculations. Top panel: resulting zero-point energies from the calculations of the lower panel. All values in cm^{-1}.

C. Optimal structures and quantum effects

In order to further investigate the quantum effects in the $CO(He)_n$ clusters, we carried out SIMPLEX optimizations[70] to find the ''classical'' optimal structures for such aggregates. In Fig. 11 we report the results of our calculations in terms of conventional bonding pictures with spheres describing the localized atoms. It is important to note at this point that we actually found several different structures for the same value of n which had total energies values below those of the ground-state energy obtained from the DMC calculations, a rather common property for rare-gas clusters.[71] Such effects originate from the highly delocalized nature of the solvent bound states in the case of helium atoms. It is instructive to compare the SIMPLEX structures, shown in Fig. 11, and the DMC results from before. One clearly sees some analogy there between classical and quantum geometries in the sense that the SIMPLEX calculations also provide clusters in which the helium atoms are located at the oxygen side, but obviously this picture does not manage to be realistic when comparing it with the DMC results that yield instead very diffuse density distributions in which a fixed geometry completely loses physical meaning. This is further proof of the fact that the vdW clusters are not realistically described unless one takes into account quantum effects. The presence, for a given number of solvent atoms, of several cluster structures, that lie very close in energy, and are separated by very small energy barriers, makes the classical picture of the clamped nuclei in the Born–Oppenheimer approximation very strongly dependent on the aggregate's temperature-annealing history. On the other hand, the quantum treatment using DMC calculations provides a more appealing physical description. This point can be demonstrated by looking at Fig. 12, in which we report the zero-point energy (ZPE) computed for the present clusters. One clearly sees that the ZPE plays a very important role in their global energetics, representing about 70% of the total binding energy. One should also note that the SIMPLEX minimization is not really reliable as it provided some total energies that, for $n=11$ and 12, were below the DMC energies, a further sign of the presence of too many equivalent structures and of the inefficiency of the simple SIMPLEX approach to reach the absolute minimum geometry.

V. CONCLUSIONS

Pairwise additive intermolecular PES for $CO(He)_n$ clusters, $n=1-12$, has been constructed from higly accurate He–He interaction[67] and anisotropic CO–He potential obtained by a recently developed treatment which combines density functional theory (DFT) with the long-range dispersion interaction.[57] As discussed in Ref. 57 this approach indicates that the use of DFT calculations yields a final PES (HHSD) which is remarkably close to the best MC-SCF results[38–40] that are obtained with a greater computational effort and to the semiempirical potential optimized to reproduce the infrared spectra of the CO–He complex.[37]

Since the CO–He potential depends on the vibrational quantum number of CO, we have followed the adiabatic treatment of Ref. 30 to investigate the energies and the structures for $CO(He)_n$ clusters in the CO vibrational state $v=0$ using the diffusion Monte Carlo (DMC) method. We have analyzed the relative stability of clusters of different size and the distributions of He atoms around the CO molecule. The comparison with the optimal structures obtained by SIMPLEX minimization[70] was also reported.

We have then shown that, in such van der Waals clusters with several shallow minima separated by low isomerization barriers, the wave function associated with the ground bound state exhibits significant amplitude values for configurations which are spatially and energetically far from the equilibrium geometry. As a result, the global minimum of the full interaction no longer defines uniquely the structure of the complex and indeed, the very notion of a molecular structure which would be described by the usual representation in terms of clamped nuclei and localized bonds, certainly a cornerstone of conventional chemistry, becomes ambiguous and has to be used with caution.

[1] F. Luo, G. C. Mcbane, G. Kim, C. F. Giese, and R. W. Gentry, J. Chem. Phys. **98**, 3564 (1993).
[2] W. Schollkopf and J. P. Toennies, Science **266**, 1345 (1994).
[3] K. B. Whaley, Int. Rev. Phys. Chem. **13**, 41 (1994).
[4] D. M. Brink and S. Stringari, Z. Phys. D: At., Mol. Clusters **15**, 257 (1990).
[5] P. Sindzingre, M. L. Klein, and D. M. Ceperley, Phys. Rev. Lett. **63**, 1601 (1989).
[6] M. V. Ramakrishna and K. B. Whaley, Phys. Rev. Lett. **64**, 1126 (1990).
[7] J. Gspann and H. Vollmar, J. Chem. Phys. **73**, 1657 (1980).
[8] A. Scheidemann, J. Northby, and J. P. Toennies, Phys. Rev. Lett. **64**, 1899 (1990).
[9] H. Buchenau, E. L. Knuth, J. Northby, J. P. Toennies, and C. J. Winkler, J. Chem. Phys. **92**, 6875 (1990).
[10] S. Grebenev, J. P. Toennies, and A. Vilesov, Science **279**, 2083 (1998).
[11] M. Hartmann, F. Mielke, J. P. Toennies, A. Vilesov, and G. Benedek, Phys. Rev. Lett. **76**, 4560 (1996).
[12] M. C. Chan, P. A. Block, and R. E. Miller, J. Chem. Phys. **102**, 3993 (1995).
[13] M. Kofranek, A. Karpfen, and H. Lischka, Chem. Phys. **113**, 53 (1987).
[14] R. Frochtenicht, J. P. Toennies, and A. Vilesov, Chem. Phys. Lett. **229**, 1 (1994).
[15] A. Scheidemann, B. Schilling, and J. P. Toennies, J. Phys. Chem. **97**, 2128 (1993).
[16] S. Goyal, D. L. Schutt, and G. Scoles, Phys. Rev. Lett. **69**, 933 (1992).
[17] M. V. Ramakrishna and K. B. Whaley, J. Chem. Phys. **93**, 6738 (1990).
[18] A. McIlroy, R. Lasacola, C. M. Lovejoy, and D. J. Nesbitt, J. Phys. Chem. **95**, 2636 (1991).
[19] E. Krotscheck and S. A. Chin, Chem. Phys. Lett. **227**, 143 (1994).
[20] S. Leutwyler and J. Bösinger, Chem. Rev. **90**, 489 (1990).
[21] S. Leutwyler and J. Jortner, J. Phys. Chem. **91**, 5558 (1987).
[22] E. R. Bernstein, in *Studies in Physical and Theoretical Chemistry, Vol. 68, Atomic and Molecular Clusters*, edited by E. R. Bernstein (Elsevier, Amsterdam, 1990).
[23] S. Goyal, G. N. Robinson, D. L. Schutt, and G. Scoles, J. Phys. Chem. **95**, 4186 (1991).
[24] R. C. Cohen and R. J. Saykally, J. Phys. Chem. **96**, 1024 (1992).
[25] R. Kosloff, A. Hammerich, and M. A. Ratner, in *Large Finite Systems*, edited by J. Jortner, A. Pullman, and B. Pullman (Reidel, Dordrecht, 1987).
[26] T. R. Horn, R. B. Gerber, and M. A. Ratner, J. Chem. Phys. **91**, 1813 (1989).
[27] Z. Bačić, M. Kennedy-Mandziuk, J. W. Moskovitz, and K. E. Schmidt, J. Chem. Phys. **97**, 6472 (1992).
[28] R. N. Barnett and K. B. Whaley, J. Chem. Phys. **96**, 2953 (1992).
[29] R. N. Barnett and K. B. Whaley, J. Chem. Phys. **99**, 9730 (1993).
[30] D. Blume, M. Lewerenz, F. Huisken, and M. Kaloudis, J. Chem. Phys. **105**, 8666 (1996).
[31] P. Hohenberg and W. Kohn, Phys. Rev. **136**, B864 (1964); W. Kohn and L. J. Sham, Phys. Rev. A **140**, 1133 (1965).
[32] G. Green and P. Thaddeus, Astrophys. J. **205**, 766 (1976).
[33] L. D. Thomas, W. P. Kramer, and G. H. F. Diercksen, Chem. Phys. **51**, 131 (1980).
[34] F. A. Gianturco, N. Sanna, and S. Serna-Molinera, J. Chem. Phys. **98**, 3833 (1993).
[35] F. A. Gianturco, N. Sanna, and S. Serna-Molinera, Mol. Phys. **81**, 421 (1994).
[36] E. C. Chuaqui, R. J. Le Roy, and A. R. W. McKellar, J. Chem. Phys. **101**, 39 (1994).
[37] R. J. Le Roy, C. Bissonette, T. H. Wo, A. K. Dham, and W. J. Meath, Faraday Discuss. Chem. Soc. **97**, 81 (1994).
[38] B. Kukawska-Tarnawska, K. Olzewiski, and G. Chalasisnski, J. Chem. Phys. **101**, 4964 (1994).
[39] F. M. Tao, R. C. Cohen, and W. Klemperer, J. Chem. Phys. **101**, 8680 (1994).
[40] R. Moszynski, T. Korona, P. E. S. Wormer, and A. van der Avoird, J. Chem. Phys. **103**, 321 (1995).
[41] T. Ziegler, Chem. Rev. **91**, 651 (1991).
[42] R. G. Parr and W. Yang, *Density Functional Theory of Atoms and Molecules* (Oxford University Press, Oxford, 1989).
[43] S. Lundquist and N. H. March, *Theory of Inhomogeneous Electron Gas* (Plenum, New York, 1989).
[44] *Density Functional Methods in Chemistry*, edited by J. Labonowski and J. Andzelm (Springer, Heidelberg, 1991).
[45] A. D. Becke, J. Chem. Phys. **98**, 1372 (1993).
[46] A. D. Becke, J. Chem. Phys. **98**, 5648 (1993).
[47] J. P. Perdew, M. Ernzerhof, and K. Burke, J. Chem. Phys. **105**, 9982 (1996).
[48] C. Adamo and V. Barone, Chem. Phys. Lett. **274**, 242 (1996).
[49] C. Adamo and V. Barone, J. Chem. Phys. **110**, 6158 (1999).
[50] J. Harris, Phys. Rev. A **29**, 1648 (1988).
[51] O. Gunnarsson and B. I. Lundquist, Phys. Rev. B **13**, 4274 (1976).
[52] J. C. Slater, *Self-Consistent Field of Molecules and Solids* (McGraw-Hill, New York, 1974).
[53] S. M. Vosko, L. Wilk, and M. Nusair, Can. J. Phys. **58**, 200 (1980).
[54] T. H. Dunning, Jr., J. Chem. Phys. **90**, 1007 (1989); D. E. Wong and T. H. Dunning, Jr., J. Chem. Phys. **98**, 1358 (1993).
[55] A. J. Stone, *Intermolecular Forces* (Clarendon, Oxford, 1996).
[56] G. A. Parker and R. T. Pack, J. Chem. Phys. **69**, 3268 (1978).
[57] F. A. Gianturco, F. Paesani, M. L. Laranjeira, M. A. Cunha, V. Vassilienko, A. G. Shashkov, and F. Zolotoukhina, Mol. Phys. **92**, 957 (1997); F. A. Gianturco, F. Paesani, M. L. Laranjeira, V. Vassilienko, M. A. Cunha, A. G. Shashkov, and F. Zolotoukhina, *ibid.* **94**, 605 (1998).
[58] F. A. Gianturco, F. Paesani, M. L. Laranjeira, M. A. Cunha, and V. Vassilienko, J. Chem. Phys. **110**, 7832 (1999).
[59] J. Anderson, J. Chem. Phys. **63**, 1499 (1975).
[60] B. L. Hammond, W. A. Lester, Jr., and P. J. Reynolds, *Monte Carlo Methods in Ab Initio Quantum Chemistry* (World Scientific, Singapore, 1994).
[61] D. M. Ceperley and B. Alder, Science **231**, 555 (1986); S. A. Chin, Phys. Rev. A **42**, 6991 (1990); M. A. Suhm and R. O. Watts, Phys. Rep. **204**, 293 (1991); W. A. Lester, Jr., and B. L. Hammond, Annu. Rev. Phys. Chem. **41**, 283 (1990).
[62] P. J. Reynolds, D. M. Ceperley, B. J. Alder, and W. A. Lester, Jr., J. Chem. Phys. **77**, 5593 (1982).
[63] C. J. Umrigar, M. P. Nightingale, and K. J. Runge, J. Chem. Phys. **99**, 2865 (1993).
[64] K. E. Schmidt and D. M. Ceperley, in *The Monte Carlo Method in Condensed Matter Physics*, Topics in Applied Physics, edited by K. Binder (Springer, New York, 1992) Vol. 71; D. M. Ceperley and M. H. Kolos, in *Monte Carlo Methods in Statistical Physics*, Topics in Current Physics, edited by K. Binder (Springer, New York, 1986), Vol. 7.
[65] S. Liu, Z. Bačić, J. W. Moskowitz, and K. E. Schmidt, J. Chem. Phys. **100**, 7166 (1994).
[66] F. Paesani and F. A. Gianturco (unpublished).
[67] R. A. Aziz and M. J. Slaman, Mol. Phys. **61**, 1487 (1987).
[68] P. Huxley and J. N. Murrell, J. Chem. Soc., Faraday Trans. 2 **79**, 323 (1983).
[69] F. Paesani, F. A. Gianturco, M. Lewerenz, and J. P. Toenniess, J. Chem. Phys. **111**, 6897 (1999).
[70] W. H. Press, B. P. Flannery, S. A. Teukolsky, and W. T. Vetterling, *Numerical Recipes in Fortran*, 2nd ed. (Cambridge University Press, Cambridge, 1992).
[71] D. J. Wales and J. P. K. Doyl, J. Chem. Phys. **101**, 5111 (1997).